Investigation of Reverse ElectroDialysis Units by Multi-Physical Modelling

L. Gurreri, F. Santoro, G. Battaglia, A. Cipollina, A. Tamburini*, G. Micale, M. Ciofalo
Dipartimento dell'Innovazione Industriale e Digitale (DIID) – Ingegneria Chimica, Gestionale, Informatica, Meccanica, Università degli Studi di Palermo (UNIPA) – viale delle Scienze Ed. 6, 90128 Palermo, Italy.
*e-mail: alessandro.tamburini@unipa.it

Abstract: Reverse electrodialysis (RED) is an electrochemical membrane process that converts the salinity gradient energy between two solutions into electric current, by using ion exchange membranes. A novel multi-physical approach for RED modelling is proposed. 2-D simulations of one cell pair with *tertiary current distribution* (Nernst–Plank equation and local electroneutrality) were performed. Moreover, the Donnan exclusion theory was implemented for simulating double layer phenomena. Transport phenomena and electrochemical behavior were well described. The influence of membrane/channel configuration, dilute concentration and feeds velocity on the process performance was assessed. For a dilute concentration ≤ 0.01M, stacks with profiled membranes reached lower resistances and higher net powers (up to 4.4 W/m^2) with respect to stacks with empty channels, thus suggesting that only in some cases the profiles lead to a performance enhancement.

Keywords: Reverse electrodialysis, multi-physics, profiled membranes, spacers.

1 Introduction

In the last decades, energy issues related to the increasing demand and to the pollution encouraged research into the study of alternative sources. Salinity gradient is virtually a huge renewable source, with a global theoretical power of 2.6 TW from seawater-river water mixing [1]. Moreover, salinity gradient is much less subjected to time fluctuations than wind and solar energy.

Reverse electrodialysis (RED) is an electrochemical membrane process that converts directly the chemical energy due to the salinity gradient between two solutions into electric energy. This technology is based on the use of ion exchange membranes (IEMs). The *cell pair* is the repeating element of the RED stack, and is composed by: anionic exchange membrane (AEM), concentrate compartment (CONC), cationic exchange membrane (CEM), and dilute compartment (DIL) [2–4]. The compartments have thickness of ~100-500 μm and are built by net spacers interposed between flat membranes, or by the profiles of profiled membranes [5].

The co-ion exclusion of the membranes gives rise to an electric double layer at each IEM-solution interface, where the chemical potential gradient is counterbalanced by the electric potential gradient (*Donnan potential*), so that the net flux is nil (ideally) [6]. Therefore, each IEM is subject to a voltage, referred to as *membrane potential*. The sum of the contributions of all the IEMs of a stack is the open circuit voltage (OCV).

The end compartments are fed by the electrode rinse solution and provided with electrodes connected each other by an external circuit with an electrical load. When the circuit is closed the voltage at the electrodes triggers redox reactions, with a subsequent flux of electrons (i.e. an electrical current) in the external circuit and ions fluxes within the stack. The co-ion exclusion of the IEMs produces a selective mass transport: cations move through CEMs and anion through AEMs, from each concentrate channel towards the two neighboring dilute ones. The voltage over the stack and, thus, over the external load will be given by the OCV minus the voltage loss due to the internal resistance of the stack.

Several works based on the Nernst–Planck approach and the electroneutrality condition have been carried out for electrodialysis (ED), and only a few specific works for RED. However, some simplifying assumptions have been done: only 1-D or 2-D simulations have been carried out, convection has been considered only in some cases, the presence of either spacers or membrane profiles has been simulated few times, and all the cell pair components have been rarely simulated.

Some models were implemented with COMSOL Multiphysics. Among these works, Brauns [7] implemented a simplified 2-D model of RED modules, based on a convective-diffusive

transport equation solved in a domain composed by two half channels provided with spacers. Only one species was simulated, thus inside the membrane with homogeneous distribution of fixed charges there is no concentration gradient and only electromigration occurs. In the expression of this flux, the potential difference over the membrane expressed by the Nernst law was inserted; therefore, the membrane was excluded from the domain and was simulated in a simplified way by applying a boundary condition at the membrane-solution interfaces.

Jeong et al. [8] proposed a more complete numerical model, although still based on several simplifications. By combining the Nernst–Planck equations of the two ionic species, the convective-diffusion equation of the electrolyte was obtained in order to compute the concentration field. Potential and current density fields were also computed. A cell pair of 0.4 m long empty channels was simulated in 2-D, membranes were not included in the computational domain, but were modelled by imposing boundary conditions. The side ends of the domain were placed at half of the channel width, with the boundary conditions of velocity and concentration gradients equal to zero and a fixed electric potential.

Tadimeti et al. [9] developed a similar model experimentally validated for ED devices in order to investigate the effect of spacer/corrugations in one channel. Membranes were included in the computational domain, but the current density was simply expressed as minus the conductivity times the potential gradient, by neglecting the effect of the concentration variations.

This work aims to develop a more complete modelling tool for RED systems, able to describe physically the transport phenomena within the cell pair and to predict the performance of a RED stack. In particular, fluid dynamics and ionic transport have been simulated in 2-D at small scale within the cell pair, including membranes; then, the electric power delivered by a stack to an external load has been computed, thus giving important information for the optimization of stack and operating conditions.

2 Physical and Numerical Model

2.1 Governing Equations

The model was implemented in COMSOL Multiphysics. *Laminar Flow* and *Tertiary Current Distribution* models were adopted. Fluid dynamics equations at steady state were:

- continuity equation

$$\vec{\nabla}\rho\vec{u} = 0 \quad (1)$$

- momentum equation

$$\vec{u}\vec{\nabla}\rho\vec{u} = -\vec{\nabla}p + \vec{\nabla}\mu\vec{\nabla}\vec{u} \quad (2)$$

where ρ is density, $\vec{u}$ is velocity vector, p is pressure, μ is dynamic viscosity.

The *Tertiary Current* distribution contains different equations:

- Nernst-Planck equation for ion flux $\vec{N_i}$

$$\vec{N_i} = \left(-D_i\vec{\nabla}c_i - z_i u_i F c_i\vec{\nabla}\phi\right) + \vec{u}c_i \quad (3)$$

where the subscript i indicates the ionic species, D_i is the diffusion coefficient, c_i is the ion concentration, z_i is the valence, u_i is the mobility, F is the Faraday's constant and ϕ is the electric potential;

- mass balance

$$\vec{\nabla}\vec{N_i} = R_i \quad (4)$$

where R_i is the production term, equal to zero in our case;

- electroneutrality

$$\sum z_i c_i = 0 \quad (5)$$

inside the membrane, z_i and c_i refer also to the fixed charges;

- current density $\vec{\imath}$

$$\vec{\imath} = F\sum_i z_i\vec{N_i} \quad (6)$$

- current density balance

$$\vec{\nabla}\vec{\imath} = F\sum z_i R_i + Q_i \quad (7)$$

where Q is a source or sink, (zero in our case).

Inside non-conductive elements which simulate net spacers, current density and electric potential are related by the Ohm's law

$$\vec{\imath} = -\sigma\nabla\phi \quad (8)$$

where σ is the conductivity, set very low.

2.2 Equivalent Electrical Circuit of a Stack and Net Power Output

Figure 1 shows a sketch of the equivalent electrical circuit used. By linking the distributed values of current density and electric potential with the quantities of the external circuit, and adding the algebraic equations of the external circuit, one can obtain (i) the boundary conditions for current density and electric potential and (ii) the calculation of the power output. The voltage over the cell pair simulated is calculated as the difference between the average values of electric potential at the external lateral boundaries

$$E_{cp} = \bar{\phi}_{AEM\_right} - \bar{\phi}_{AEM\_left} \quad (9)$$

The average current density is:

$$\bar{\imath} = \frac{1}{l}\int i\, dl \qquad (10)$$

where l denotes the length of the 2-D domain simulated (1.2 mm). This current density is supposed to be maintained for a stack in lab-scale, in which, thus, the electric current is

$$I = \bar{\imath} A_{stack} \qquad (11)$$

where A_{stack} is

$$A_{stack} = LW \qquad (12)$$

L and W being the effective length and width of the channel (both 0.096 m in the simulations shown in this work).

By the external circuit, the electric current and the cell pair voltage are related as

$$I = \frac{NE_{cp}}{R_{blank} + R_{ext}} \qquad (13)$$

where N is the number of cell pairs (10 in the simulations showed in this paper), R_{blank} is the resistance of the electrodic compartments, which were not simulated, and was fixed equal to 1.02 Ω (from experimental results) and R_{ext} is the resistance of the external load (variable input parameter). The voltage over the stack was

$$E_{stack} = IR_{ext} \qquad (14)$$

The cell pair resistance was calculated as

$$R_{cp} = \frac{E_{OCV,cp} - E_{cp}}{I} \qquad (15)$$

where $E_{OCV,cp}$ is the open circuit voltage of the cell pair, computed by simulation with $R_{ext} \rightarrow \infty$ Ω.

The gross power density *per membrane area* produced by the stack was

$$P_{d,gross} = E_{stack}\bar{\imath} \qquad (16)$$

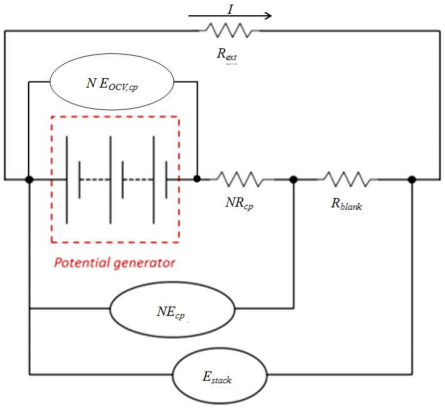

Figure 1. Equivalent electrical circuit.

The power density consumed for pumping the solutions was

$$P_{d,pump} = \frac{\Delta p_{CONC} Q_{CONC} + \Delta p_{DIL} Q_{DIL}}{A} \qquad (17)$$

where Δp is the pressure drop in the channel, and Q the is the volumetric flow rate, calculated as:

$$\Delta p = \frac{(p_{inlet} - p_{outlet})_L}{l} \qquad (18)$$

$$Q = uHW \qquad (19)$$

in which H is the channel height, and the other symbols have the meaning mentioned above. Finally, the net power density was

$$P_{d,net} = P_{d,gross} - P_{d,pump} \qquad (20)$$

2.3 Computational Domain, Boundary Conditions and Materials

A cell pair, representing the repeating unit, of a RED device was simulated in 2-D (see Figure 2). Electrodic compartments were not simulated. The lateral boundaries were placed in correspondence of half AEM. In order to limit the computational load, the length of the cell pair l was assumed of 1.2 mm, corresponding to two periodic geometric units of the channels either with membrane profiles or insulating spacers.

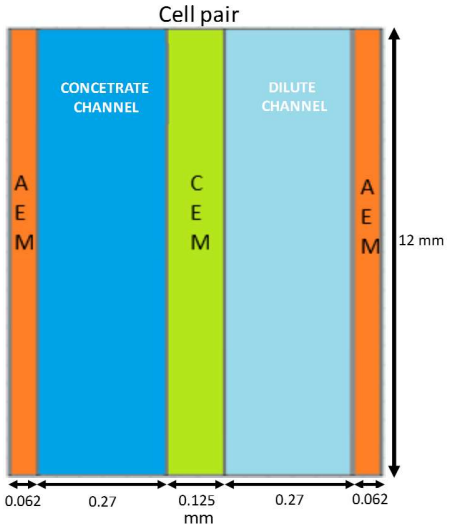

Figure 2. Computational domain.

The inlet velocities were set in the range 0.3-5 cm/s in co-current flow, and the outlet pressures were set at 1 atm. The inlet concentration was set at 4 M for the concentrate channel and in the range 0.005-0.5 M in the dilute channel. The choice of the concentrations was made in order simulate optimal conditions for the power output, with possible applications in areas where concentrate brines are available (salt works, very salty lakes, industrial sites) or for a closed loop, where the

solutions are regenerated from low grade heat in a range of temperature between 50 °C and 100 °C (e.g. solar and geothermal energy or waste heat).

The lateral boundaries were set as periodic, ensuring that at the two boundaries all variables assumed the same distribution and that the electric potential, however, was different due to the generation and loss terms inside the domain. Moreover, the current density was set with the condition on the average value of eqs. (11)-(13).

At the IEM-solution interfaces, the no slip and the Donnan electrochemical equilibrium conditions were set. Of course, in the present simulations, the scale is much larger than that of the double layer, thus immediate jumps of electric potential and concentrations were imposed at these interfaces. The values at the membrane-side were computed from the following formulae, by assuming activity coefficients equal to 1:

$$\varphi_{IEM} = \varphi_{sol} + \frac{RT}{z_{counter}F} ln \frac{c_{counter,sol}}{c_{counter,IEM}} \quad (21)$$

$$c_{co,IEM} = \frac{1}{2}\left(\sqrt{c_{fix}^2 + 4c_{co,sol}c_{counter,sol}} - c_{fix}\right) + \alpha c_{fix} \quad (22)$$

where α is a correction parameter [10].

NaCl aqueous solutions were simulated, by assuming that the fluids were Newtonian and incompressible. The ion mobility in solution was computed by the Nernst-Einstein equation:

$$u_i = \frac{D_i}{RT} \quad (23)$$

Membranes were assumed homogeneous and isotropic and were simulated as electrolytic solutions with nil flow field. Due to the lack of direct measurements, ionic diffusivity and mobility in membrane were obtained by model calibration with experimental data. In the membrane domains one additional variable was implemented, i.e. the concentration of fixed charges. The values of this quantity were set as homogeneous and equal to 4266.7 mol/m^3 for the AEM and 4833.3 mol/m^3 for the CEM (from experimental data). The diffusion coefficient and the mobility of the fixed charges were set at zero.

All the simulations were run at the temperature of 20 °C.

2.4 Membrane/Channel Configurations

Four different configurations of cell pair were simulated: (i) flat membranes and empty (spacer-less) channels, (ii) flat membranes and non-conductive square spacers, (iii) flat membranes and non-conductive circular spacers, (iv) profiled (square) membranes (see Figure 3). The distance between two obstacles was 600 μm.

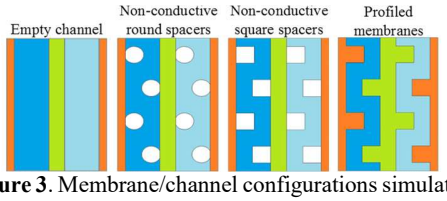

Figure 3. Membrane/channel configurations simulated.

2.5 Mesh and Solver

Hybrid meshes were used (see the example of Figure 4). They were composed by quadrilateral elements in correspondence of the boundaries and triangular elements elsewhere. Grid independence was preliminarily addressed, and a mesh with a total number of elements of ~80,000 was chosen.

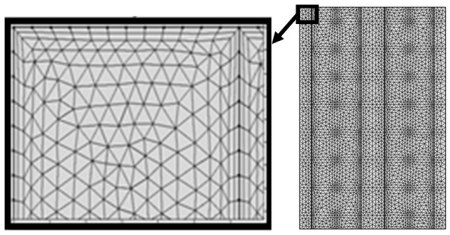

Figure 4. Discretization of the computational domain. The example refers to the case of empty channels.

Steady state conditions were simulated (stationary solver). The numerical solution was structured in three steps: the first step solved the fluid dynamics (*laminar flow*); the second step solved the electrochemistry (*Nernst-Planck*), by using the velocity field found by the first step; finally, the third step calculated all physics together. The fully coupled direct solver MUMPS was used for each step.

3 Results and discussion

3.1 Distribution of the Main Quantities

Fluid dynamics and transport phenomena are very important, and are notably affected by the geometry. Figure 5 shows the velocity maps for the various geometries simulated. At the very low Reynolds numbers typical for RED channels (< 10) any chaotic component is absent. Within

empty channels the flow is parallel and the velocity has a parabolic profile. When obstacles are present, velocity components perpendicular to the membranes arise, i.e. the flow path is tortuous. As a consequence, higher pressure drops are expected. On the other hand, a mixing enhancement is likely, although stagnant regions in the proximity of the obstacles can affect negatively this aspect. Finally, some small differences are caused by the obstacle shape.

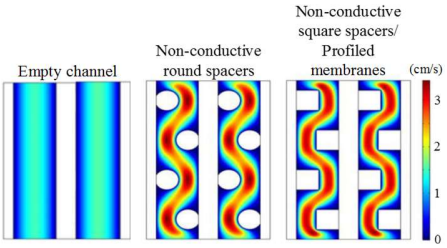

Figure 5. Velocity map for the different configurations simulated, at an inlet velocity of 1 cm/s.

Transport phenomena of ions involve the whole cell pair, occurring both in solution and in membrane. Figure 6 shows an example of concentration profiles predicted in the case of empty channels. Double layer phenomena are simulated by eq. (22) as sudden jumps of concentration at the IEM-solution interface. Because of the electroneutrality condition (eq. (5)), in solution the concentrations of Na^+ and Cl^- are equal, while in membrane they differ of a quantity equal to concentration of the fixed charges. The co-ions concentration inside the membranes is not negligible at all, due to the high salt concentration of the concentrate solution.

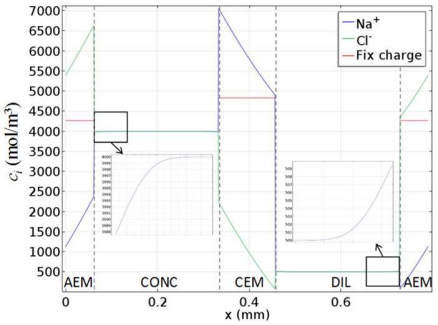

Figure 6. Concentration profiles within the cell pair with empty channels, fed by 4M-0.5M solutions at 1 cm/s. Simulation at maximum gross power density conditions ($R_{ext} \approx 2\ \Omega$). The values are taken along a horizontal midline.

Figure 6 shows also concentration polarization phenomena within the fluid domains. At open circuit, as the membranes are not perfectly permselective, a diffusive transport takes place, thus generating concentration gradients. At closed circuit, a current passes through the stack and is carried in solution in a similar amount by cations and anions (transport numbers $\approx$ 0.5), and in membrane almost exclusively by counter-ions (transport number close to 1), thus the total flux is maintained constant by a diffusive flux in solution (boundary layer). Finally, the concentration gradients cause a decrease of chemical potential difference over the membrane, and thus of membrane potential.

This is computed by the sudden jumps at the IEM-solution interfaces (eq. (21)) shown in Figure 7, which reports the potential profiles at different external loads. In particular, the IEM-CONC interfaces cause a loss of voltage, while the IEM-DIL interfaces produce a larger gain of voltage. The effect of the concentration polarization is an increase of the losses and, mostly, a reduction of the gains.

At open circuit, no electric current circulates, thus there are no voltage losses; the electric potential is flat both in solution and in membrane (since the diffusion coefficients were set at the same values for counter- and co-ions by model calibration, no diffusive potential is generated within the membrane). Note that the membrane permselectivity is given by the ratio between the actual membrane potential and the membrane potential obtainable with $c_{counter,sol} = c_{fix}$. At closed circuit, an electric current passes through the cell pair and the potential exhibits some losses. They are the largest ones in short-cut conditions, i.e. when the maximum current is circulating. The maximum gross power density is obtained when the stack voltage is equal to OCV/2, corresponding to an external resistance equal to the internal one (actually, non ohmic phenomena may cause a small deviation).

The voltage drop is significant within the membranes and, although lower, within the 0.5M dilute solution. Conversely, the electric potential is constant within the 4M concentrate solution. This behaviour is due to the different values of conductivity, which is given by

$$k = F^2 \sum_i z_i^2 u_i c_i \qquad (24)$$

Note that the large variation of concentration inside the membrane caused a significant

variation of conductivity, thus giving a curvature to the electric potential profile.

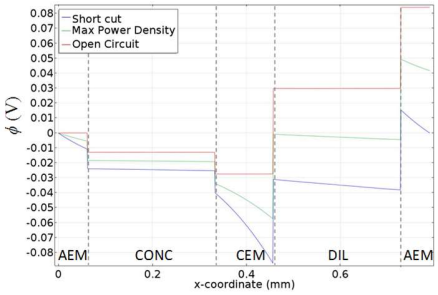

Figure 7. Potential profile within the cell pair with empty channels, fed by 4M-0.5M solutions at 1 cm/s, at different external loads. R_{blank} was set equal to zero in order to visualize inside the cell pair all the internal loss. The values are taken along a horizontal midline.

It is very interesting also the effect of the conductivity on the current density distribution in more complex geometries. Figure 8 shows the current density maps and streamlines for a cell pair fed by c_{CONC} = 4M and c_{DIL} = 0.01, 0.05 and 0.1M. When the profiles are immersed into a very conductive solution as the 4M CONC, they exhibit an almost null current density and are bypassed by the streamlines. Conversely, when the profiles are immersed into a less conductive solution as the 0.01M DIL, they are crossed by a higher current density. A concentration of 0.05M is sufficient to have a conductivity higher than the present membranes, and a concentration of 0.1M makes negligible the current density inside the profiles. Therefore, the features of membranes and solutions affect significantly the usefulness of the profiles for making increase the active area and reducing the stack resistance.

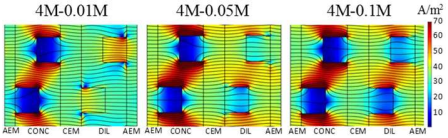

Figure 8. Current density distribution within the cell pair with profiled membranes, fed by 4M concentrate solution and various dilute solutions at 1 cm/s. Simulations at maximum $P_{d,gross}$ conditions.

3.2 Sensitivity Analysis

Several simulations were performed in order to investigate the influence of membrane/channel configuration, dilute concentration and feeds velocity on electrical resistance, OCV, gross power density and net power density.

Figure 9 reports the cell pair resistance (R_{cp}) for different dilute concentrations and membrane/channel configurations. This is the total resistance, due both to ohmic and non-ohmic phenomena. Non-ohmic losses of voltage are caused by concentration variations at the IEM-fluid interface with respect to the inlet concentration (concentration polarization and variation along the flow direction). At 1 cm/s non-ohmic resistances were about 10% of R_{cp}.

As c_{DIL} increases, R_{cp} decreases, due to the higher conductivity and the lower boundary layer effect [11]. With 0.005M concentration R_{cp} is about 9 times the resistance with 0.5M. Non-conductive spacers led to larger resistances almost for all the c_{DIL} values. Square spacers occupy a larger area, thus having a higher effect and causing the largest resistances. Profiled membranes are effective in reducing R_{cp} only at $c_{DIL} \leq$ 0.01M, while empty channels perform better in the case of more conductive solutions.

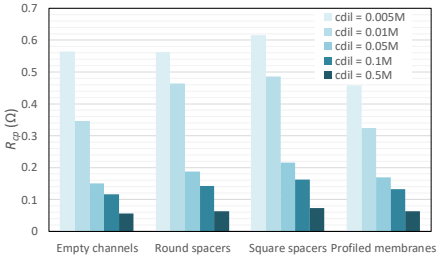

Figure 9. Cell pair resistance for different dilute concentrations and membrane/channel configurations, at the fluid velocities that maximize the net power density, and with 4M concentrate solution.

The gross power density ($P_{d,gross}$) depends on R_{cp} and also on OCV, which, in turns, is affetced strongly by the feeds concentrations. In particular, the trend of $P_{d,gross}$ with the geometry is inverted with respect to R_{cp}, while the trend of $P_{d,gross}$ with c_{DIL} has a maximum. This features are reflected into the $P_{d,net}$, which is also influenced by the pumping power and, thus, again by the geometry (fluid properties change only slightly with c_{DIL}).

Figure 10 reports the maximum net power densities. Among the dilute concentrations considered, the highest $P_{d,net}$ were obtained for 0.01M or 0.05M. The differences of $P_{d,net}$ among

the configurations decrease as the c_{DIL} increases. Stack with spacers were characterized by higher R_{cp} and pressure drops, thus leading to lower $P_{d,net}$, especially in the case of square shape. Profiled membranes enhanced the process performance with respect to the empty channels for $c_{DIL} \leq$ 0.01M, yielding the maximum $P_{d,net} \approx 4.4$ W/m^2.

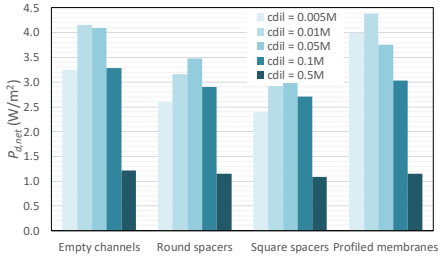

Figure 10. Maximum net power density for different dilute concentrations and membrane/channel configurations, with 4M concentrate solution

4 Conclusions

A multi-physical model of RED devices was developed. Fluid dynamics, electrochemical mass transport and double layer phenomena were modelled in the cell pair by the Nernst–Plank approach and the Donnan exclusion theory.

A sensitivity analysis of the stack performance to the stack features and operating conditions, as membrane/channel configuration, dilute concentration (concentrate fixed at 4M) and feeds velocity, was addressed.

The differences in $P_{d,net}$ among the configurations were lower as c_{DIL} increased. Cell pairs with non-conductive spacers were characterized by higher resistance (including the boundary layer resistance) and pressure drop, and thus by lower net power. The present membranes were found more conductive than solutions up to 0.01M, thus reducing the cell resistance with respect to empty channels for $c_{DIL} \leq$ 0.01M. In particular, the highest net power density of ~4.4 W/m^2 was reached by profiled membranes with c_{DIL} = 0.01M. Therefore, the effectiveness of profiled membranes for the active area increase and the stack resistance reduction depends significantly on the features of the membranes and of the solutions, and only in some conditions the profiles can enhance the stack performance. Of course, manufacturing highly conductive membranes would be important for the process optimization.

5 References

1. G.L. Wick, W.R. Schmitt, Prospects for Renewable Energy from Sea, *Mar. Technol. Soc. J.*, **11**, 16–21 (1977)
2. R.E. Pattle, Production of Electric Power by mixing Fresh and Salt Water in the Hydroelectric Pile, *Nature*, **174**, 660–660 (1954)
3. J.N. Weinstein, F.B. Leitz, Electric power from differences in salinity: the dialytic battery, *Science*, **191**, 557–559 (1976)
4. R.E. Lacey, Energy by reverse electrodialysis, *Ocean Eng.,* **7**, 1–47 (1980)
5. D.A. Vermaas, M. Saakes, K. Nijmeijer, Enhanced mixing in the diffusive boundary layer for energy generation in reverse electrodialysis, *J. Memb. Sci.*, **453** 312–319 (2014)
6. H. Strathmann, Ion-exchange membrane separation processes, first ed., Elsevier, Amsterdam, 2004
7. E. Brauns, Finite elements-based 2D theoretical analysis of the effect of IEX membrane thickness and salt solution residence time on the ion transport within a salinity gradient power reverse electrodialysis half cell pair, *Desalin. Water Treat.*, **51** 6429–6443 (2013)
8. H.-I. Jeong, H.J. Kim, D.-K. Kim, Numerical analysis of transport phenomena in reverse electrodialysis for system design and optimization, *Energy*, **68** 229–237 (2014)
9. J.G.D. Tadimeti, V. Kurian, A. Chandra, S. Chattopadhyay, Corrugated membrane surfaces for effective ion transport in electrodialysis, *J. Memb. Sci.*, **499** 418–428 (2016)
10. A.H. Galama, J.W. Post, M.A. Cohen Stuart, P.M. Biesheuvel, Validity of the Boltzmann equation to describe Donnan equilibrium at the membrane–solution interface, *J. Memb. Sci.*, **442** 131–139 (2013)
11. L. Gurreri, a. Tamburini, a. Cipollina, G. Micale, M. Ciofalo, CFD prediction of concentration polarization phenomena in spacer-filled channels for reverse electrodialysis, *J. Memb. Sci.*, **468** 133–148 (2014)

6 Acknowledgements

This work has been performed within the RED-Heat-to-Power project (Conversion of Low Grade Heat to Power through closed loop Reverse Electro-Dialysis) - Horizon 2020 programme, Grant Agreement n. 640667, http://www.red-heat-to-power.eu.